Science Bulletin 64 (2019) 540–546

Contents lists available at ScienceDirect

Science Bulletin

journal homepage: www.elsevier.com/locate/scib

Science Bulletin
www.scibull.com

Article

Flexible and transparent graphene/silver-nanowires composite film for high electromagnetic interference shielding effectiveness

Ning Zhang [a,1], Zhe Wang [a,1], Rongguo Song [a], Qianlong Wang [b], Hongye Chen [a], Bin Zhang [a], Haifei Lv [a], Zhi Wu [a], Daping He [a,*]

[a] Hubei Engineering Research Center of RF-Microwave Technology and Application, School of Science, Wuhan University of Technology, Wuhan 430070, China
[b] Shenzhen Institute of Advanced Graphene Application and Technology (SIAGAT), Shenzhen 518106, China

ARTICLE INFO

Article history:
Received 7 January 2019
Received in revised form 27 February 2019
Accepted 4 March 2019
Available online 28 March 2019

Keywords:
Flexibility
Transparent
Electromagnetic interference shielding
Graphene
Silver nanowires

ABSTRACT

Herein, an efficient approach to prepare flexible, transparent, and lightweight films based on graphene nanosheets (GNS) and silver nanowires (AgNWs) for high electromagnetic interference (EMI) shielding effectiveness (SE) has been explained. High-conductive GNS were fabricated by liquid phase stripping and composited with AgNWs by a two-step spin-coating method. Owing to the high transparency, good conductivity, and homogeneous distribution of both GNS and AgNWs, the obtained GNS/AgNWs film exhibits superb EMI SE and light transmittance, yielding a significantly high EMI SE up to 26 dB in both Ku-band and K-band and light transmittance higher than 78.4%. Moreover, this GNS/AgNWs film shows good flexibility and excellent structural stability. The obtained flexible, light and transparent film could have a great potential for transparent EMI shielding and smart electronics.

1. Introduction

With the rapid development of modern electronics and wireless communication technology, the electromagnetic interference (EMI) of radio frequency radiation is becoming a new and serious global pollutant source [1–4]. More and more attention has been paid to the development of high-performance EMI shielding materials [5]. Currently, metal materials, such as copper and aluminum shrouds, are well-known and conventionally used as the EMI shielding materials, but their wide applications still suffer from poor mechanical flexibility and excessive weight [6–8], which limits their development on EMI shielding materials in biomedical and wearable electronics [9–11]. On the other hand, the high EMI shielding effectiveness (SE) in visual observation modern electronics, like electronic displays, observation windows, is very important but really difficult to obtain [12–14]. Therefore, it is highly desirable to develop a flexible, lightweight, transparent, and efficient EMI shielding material.

In the past decades, the flexible transparent conductive films, which are made by adding appropriate content of conductive components, such as carbon nanotubes (CNTs) [15–20], silver nanowires (AgNWs), and metal mesh, into the polymer film matrix [21,22], have raised great attention in flexible electronics and EMI shielding field [23]. For example, Umrao et al. [24] reported that CNTs films achieved both high EMI SE and light transmittance, but the large-scale production with high uniformity is littered with challenges [25,26]. Also, conductive metal grids with micron line width, such as AgNWs, are promising candidates for high transparent EMI shielding materials [27,28]. Jin et al. [29] used AgNWs to embed glass fiber to make reinforced transparent composite film and the EMI SE is 12.5–16 dB when the light transmittance is 80% at 8–12 GHz. The metal mesh can be fabricated on different substrates to meet the requirements of optical transmittance and EMI SE and it can be fabricated in a large area at low cost. Besides, Vishwanath et al. [30] made a metal mesh structure with the light transmittance of 88.2% and the EMI SE of 20 dB at 8–12 GHz. However, the main shielding mechanism of metal is based on reflection, which will bring profound secondary pollution to the environment. In addition, AgNWs exposed to the air are threatened by chemical attack and their lifespan are severely shortened.

More recently, the two-dimensional graphene has become a choice for manufacturing macroscale flexible conductors because of their light weight, good mechanical flexibility and high light transmittance [31–34]. It is reported that the EMI shielding mechanism of graphene nanosheets (GNS) is mainly absorption [5]. However, it is difficult to obtain high transparency and strong SE by pristine GNS. In order to further improve the EMI shielding performance, the GNS material is usually compounded with a metal

* Corresponding author.
E-mail address: hedaping@whut.edu.cn (D. He).
[1] These authors contributed equally to this work.

https://doi.org/10.1016/j.scib.2019.03.028
2095-9273/

material [35–38]. Han et al. [39] used a combination of GNS and metal mesh structure to make a film, and the EMI SE was 14.1 dB in the 12–18 GHz when the light transmittance was 90.5%. Kim et al. [23] fabricated the polymer-coated/reduced graphene oxide/silver nanowires with an EMI SE of 24.1 dB in 0.5–3 GHz and a light transmittance of 82.5%. Ma et al. [40] fabricated a polymethyl methacrylate (PMMA)/graphene/metal mesh hybrid film with the EMI SE of up to 28.9 dB at 12–18 GHz when the light transmittance was 91%. Lu et al. [41] prepared graphene/metallic mesh/transparent dielectric hybrid structure with the EMI SE of 34.5 dB at 26.5 GHz when the light transmittance was 85%. Nevertheless, the frequency bands in the previous reports need to be further broadened with simplified the sample preparation process and further improved EMI SE. Moreover, graphene produced by chemical vapor deposition (CVD) suffers from the complex preparation process and uncontrollability. And the graphene oxide cannot achieve enough high EMI SE because of low conductivity.

In this paper, a high conductive GNS, fabricated by liquid phase stripping, is introduced and composited with AgNWs by a two-step spin-coating method. The composite film shows a strong EMI SE in wide frequency range and excellent light transmittance, which are tunable by controlling the amount of the GNS. The combination of GNS and AgNWs solves the problem that a single material cannot be balanced in terms of light transmittance and EMI SE. This work will be of great significance for EMI shielding materials.

2. Experimental

2.1. Materials

GNS was synthesized from natural graphite flakes by a liquid phase stripping method [42] (the synthesizing details can be seen in Supplementary Data online). The AgNWs solution was prepared using a modified polyol method [43] (preparation details can be seen in Supplementary Data online). Norland Optical Adhesive 63 (NOA63) was purchased from Norland Products, Inc. Poly(3,4-ethylenedioxythiophene):poly(styrenesulfonate) (PEDOT:PSS) was purchased from Xi'an Polymer Light Technology Co.

2.2. Fabrication of transparent GNS/AgNWs film

The previously prepared AgNWs and GNS were separately dispersed in ethanol. The glass pieces were ultrasonically cleaned with ultra-pure water ($\sigma = 5.5 \times 10^{-6}$ S/m) and ethanol for 15 min, then dried and placed under UV light for 20 min. PEDOT:PSS was spin-coated on one side of the as-prepared glass piece at 2,500 r/min for 30 s, and then placed on a heating table at 120 °C for 20 min. The AgNWs solution was spin coated on PEDOT:PSS at the same speed and time, then heated at 150 °C for 20 min. Then, the graphene solution was spin-coated on AgNWs at 1,500 r/min for 30 s, and heated at 120 °C for 20 min. Finally, the obtained composite film was packaged with the NOA63 by spin-coating, then placed under UV light for about 2 min. Then glass piece was placed in ultra-pure water for 20 min to dissolve PEDOT:PSS and separate the glass piece from the GNS/AgNWs film. The GNS/AgNWs film characterizations are shown in Supplementary Data (online).

Among them, GNS-1L, GNS-2L and GNS-3L indicate the films with GNS of 0.8, 1.6 and 2.4 mL, respectively. AgNWs-1L, AgNWs-2L and AgNWs-3L indicate the films with AgNWs of 0.12, 0.36 and 0.6 mL, respectively. GNS/AgNWs-1L, GNS/AgNWs-2L and GNS/AgNWs-3L respectively indicate the films combining AgNWs of 0.12, 0.36 and 0.6 mL with GNS of 1.6 mL. Graphene oxide (GO)/AgNWs-1L, GO/AgNWs-2L and GO/AgNWs-3L indicate the films combining AgNWs of 0.12, 0.36 and 0.6 mL with GO of 1.6 mL, respectively.

2.3. Measure of optical transmittance

Using the same thickness of NOA63 film as a reference, the optical transmittance of the GNS/AgNWs films was measured by a UV–visible spectrophotometer (Shimadzu UV2600) in the wavelength range from 400 to 800 nm.

2.4. Measure of sheet resistance

The sheet resistance (R_s) was measured by using a four-point probe (RTS-8, Guangzhou Four Point Probe Technology Co., Ltd.). Based on the fact that NOA63 is non-conductive while both AgNWs and graphene are conductive, we measured the sheet resistance of the GNS/AgNWs film to characterize their electrical properties.

2.5. Measure of EMI SE

The EMI SE of the GNS/AgNWs film was tested by the N5247A vector network analyzer using the transmittance-reflection-load technique at both ends of the waveguide. The measured frequency ranges were Ku-band (12.4–18 GHz) and K-band (20–26 GHz) with an intermediate frequency bandwidth of 300 Hz. The sample was cut to a size slightly larger than the waveguide window ((15.799×7.899) mm^2 for Ku-band and (10.668×4.318) mm^2 for K-band), then sandwiched tightly between the two waveguides. The principle of EMI SE is explained in Supplementary Data (online).

3. Results and discussion

The GNS film, AgNWs film and GNS/AgNWs film are all produced by a spin coating method. Fig. 1 shows the specific fabrication process of the GNS/AgNWs films. Firstly, PEDOT:PSS, AgNWs, GNS and NOA63 are sequentially coated on one side of a glass piece substrate in turn. Then the glass piece is immersed in ultra-pure water to dissolve the PEDOT:PSS, and the GNS/AgNWs film is finally obtained.

In order to explore the internal structure information, GNS/AgNWs was deposited onto a silicon wafer to obtain X-ray diffraction (XRD) pattern and Raman spectrum. As shown in XRD pattern (Fig. 2a), the diffraction peak of (0 0 2) lattice plane in GNS, which is located at $2\theta = 26.33°$, indicates that interlayer spacing $d = 0.34$ nm [44]. The diffraction peaks situated at $2\theta = 37.92°$ and 44.62° represent the (1 1 1) and (2 0 0) lattice plane of AgNWs, respectively. The diffraction peak situated at $2\theta = 69.18°$ belongs to (1 0 0) lattice plane of Si substrate. These results prove the existence of GNS and AgNWs, which are in agree consistent with Raman spectra. Raman spectra of GNS/AgNWs film are shown in Fig. 2b. The D peak and G peak of GNS are located at 1,392.92 and 1,565.04 cm^{-1}, respectively. In addition, Raman peak of AgO located at 221.30 cm^{-1} can prove indirectly the existence of AgNWs [45]. The peaks lay on 517.17 and 966.31 cm^{-1} belong to Si substrate. In order to observe microscopic morphology of GNS, transmission electron microscope (TEM) images were taken. It can be found in Fig. 2c and d that there are many wrinkles on the GNS, which provide the possibility to resist bending and enhance flexibility. The normal GO with more oxygen-containing functional groups [46], is easy to be twisted by itself (Fig. 2e), increasing the sheet resistance. Therefore, the sheet resistances of GNS/AgNWs films are smaller than that of GO/AgNWs films (Fig. 2f). In theory, EMI SE of a conductive material increases with its sheet resistance R_s decreasing [47,48], which is mentioned in Supplementary Data and the experimental results in Fig. 2f verify this conclusion. Furthermore, as the number of layer increases, the corresponding sheet resistance of the film gradually decreases.

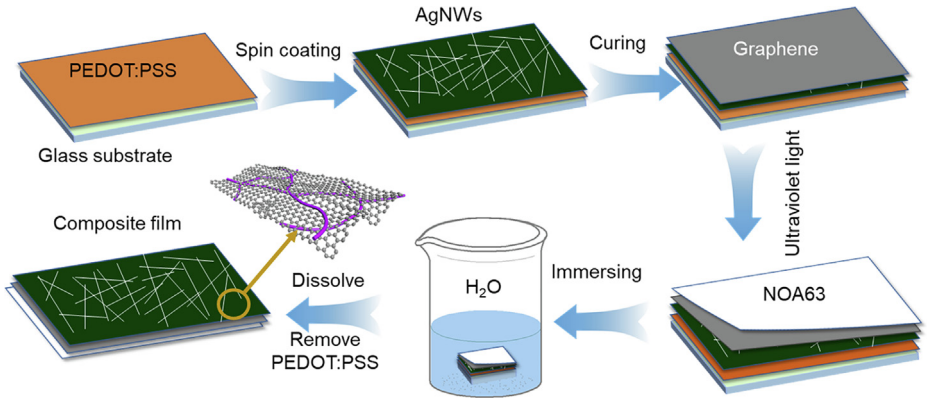

Fig. 1. (Color online) Preparation process of the GNS/AgNWs film.

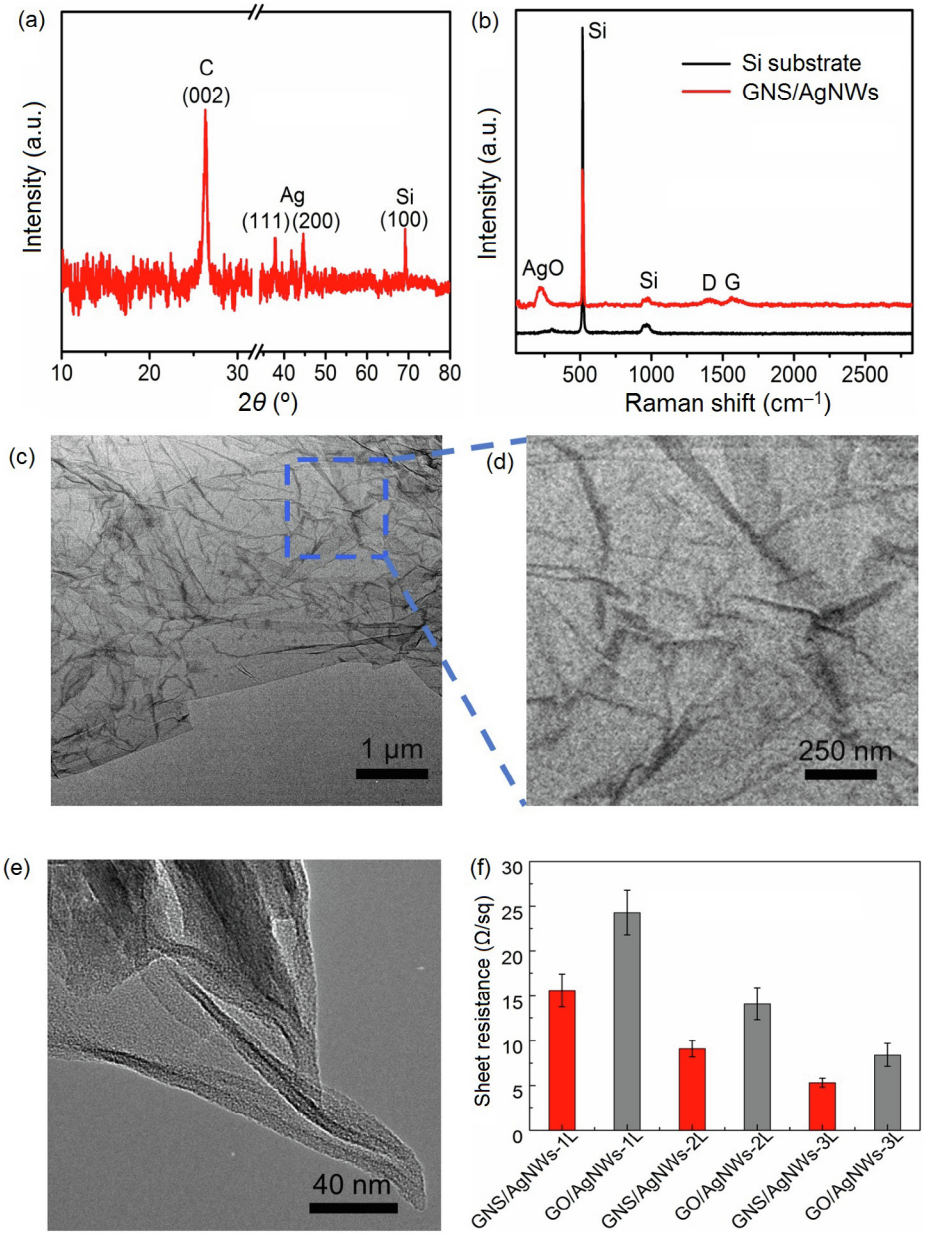

Fig. 2. (Color online) Characterizations of GNS/AgNWs films. The XRD pattern (a) and Raman spectrum (b) of the GNS/AgNWs. (c), (d) The TEM image of a GNS with many wrinkles. (e) The TEM image of the normal graphene oxide. (f) The sheet resistance of GNS/AgNWs films and GO/AgNWs films.

The light transmittance results of the GNS film, AgNWs film and GNS/AgNWs film are also investigated. As shown in Fig. 3a–c, the GNS film exhibits high light transmittance, while AgNWs film and GNS/AgNWs film show a little lower light transmittance. This can be further proved by the spectrophotometer (Shimadzu UV2600) test results. GNS-1L film has excellent light transmittance, which can reach up to 94.7% (Fig. 3d). And light transmittance value of the AgNWs-1L film can reach to 81.5% (Fig. 3e). Based on these two components, the light transmittance of the GNS/AgNWs-1L film can be up to 78.4%, which is close to that of AgNWs-1L film (Fig. 3f). Moreover, the light transmittance decreases with the content of any component increases. Scanning electron microscopy (SEM) images of the three types of films explain the difference of their light transmittance results. The light transmittance of single-layer graphene is as high as 97.3% [49], thus making GNS films have ultrahigh light transmittance (Fig. 3g). In terms of AgNWs, the network structure allows light to go through the mesh, making AgNWs possess good light transmittance (Fig. 3h). As for GNS/AgNWs film (Fig. 3i), GNS attaches on AgNWs network, and blocks some meshes of the AgNWs, decreasing light transmittance a little (Fig. S1 online). In addition, we also tested light transmittance of GO/AgNWs films, which are inferior to that of GNS/AgNWs films (Fig. S2 online).

The GNS/AgNWs film with a thickness of ~ 30 μm can be folded into a zigzag shape and bent without any damage, exhibiting excellent flexibility (Fig. 4a). The relative volume resistance of the GNS/AgNWs film is maintained at 181.5 ± 0.3 Ω during bending process (Fig. S3 online). The relative volume resistance of the GNS/AgNWs film is almost unchanged during 100 times bending test with the bending angle of ~80° (Fig. S4 online). Apart from superb light transmittance and flexibility, the GNS/AgNWs films show outstanding EMI SE. As shown in Fig. 4b, when electromagnetic wave radiation goes through the GNS/AgNWs film, the attenuation of electromagnetic waves is caused by the following three scenarios: (1) reflected and attenuated on the surface of GNS/AgNWs film; (2) absorbed and attenuated gradually in the GNS/AgNWs film; (3) reflected and attenuated again and again in GNS/AgNWs film.

This EMI shielding mechanism can be proved by the EMI SE testing results. Fig. 4c shows the Network Analyzer (PNA-X, N5247A) that investigate the EMI SE of films at 12.4–18 and 20–26 GHz via the waveguide method. The inset is a partial enlarged view of the waveguide device.

Fig. 4d, e shows the EMI SE in Ku-band of the AgNWs films and GNS/AgNWs films, respectively. With the same content of AgNWs, GNS/AgNWs films possess higher EMI SE than AgNWs films. Particularly, the EMI SE of AgNWs-3L film is only 32.6 dB at maximum, while the EMI SE of GNS/AgNWs-3L film can reach up to 38.5 dB. The addition of GNS improves electrical conductivity, and two-dimensional (2D) structure of GNS can block and absorb the leakage of electromagnetic radiation through the meshes of the AgNWs. Fig. 4f shows the EMI shielding efficiency of GNS/AgNWs films is higher than that of AgNWs films at 12.4–18 GHz. At the same time, the efficiency error of the GNS/AgNWs films is lower than that of AgNWs films, exhibiting higher EMI SE stability of the GNS/AgNWs films at 12.4–18 GHz. The reflection efficiency and absorption efficiency of AgNWs films and GNS/AgNWs films

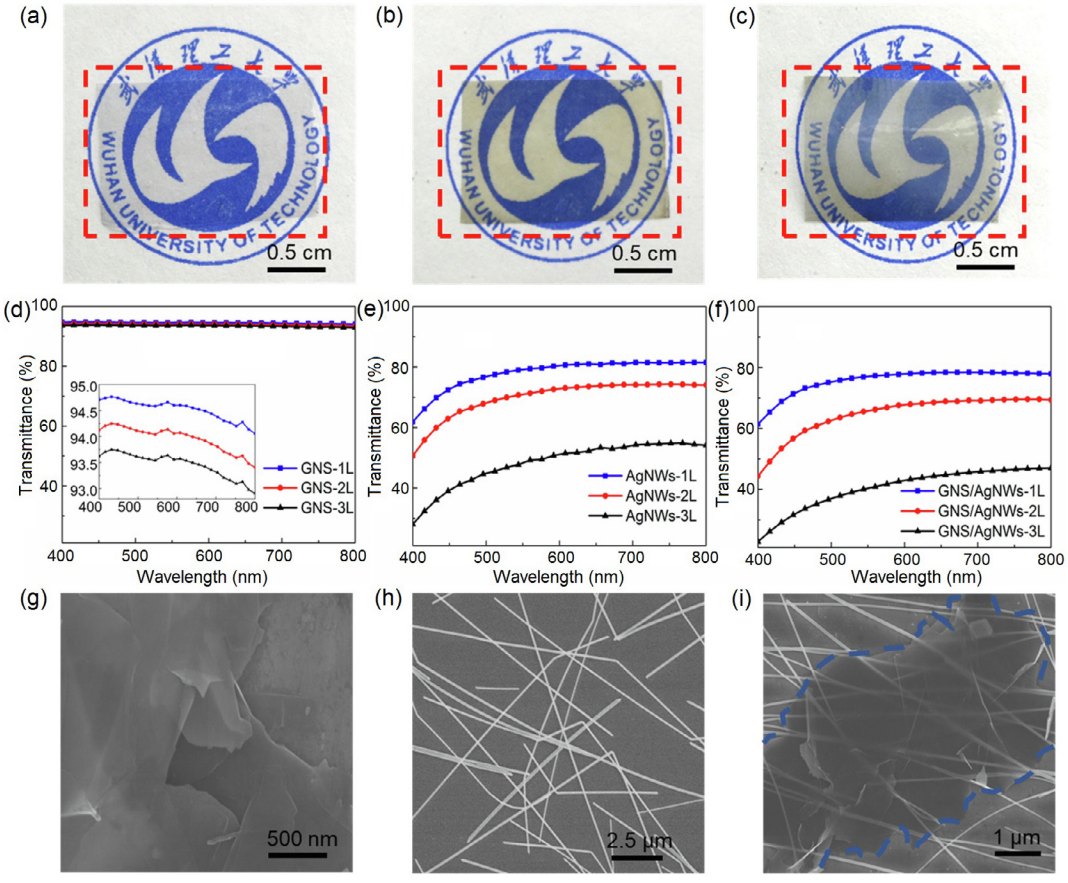

Fig. 3. (Color online) Light transmittance results and morphology of the films. The digital images of the GNS-2L film (a), AgNWs-2L film (b) and GNS/AgNWs-2L film (c), respectively. The light transmittance results of GNS films (d), AgNWs films (e) and GNS/AgNWs films (f) at 400–800 nm, respectively. The inset in (d) is the enlarged view of the curves. The SEM image of GNS film (g), AgNWs film (h) and GNS/AgNWs film (i), respectively.

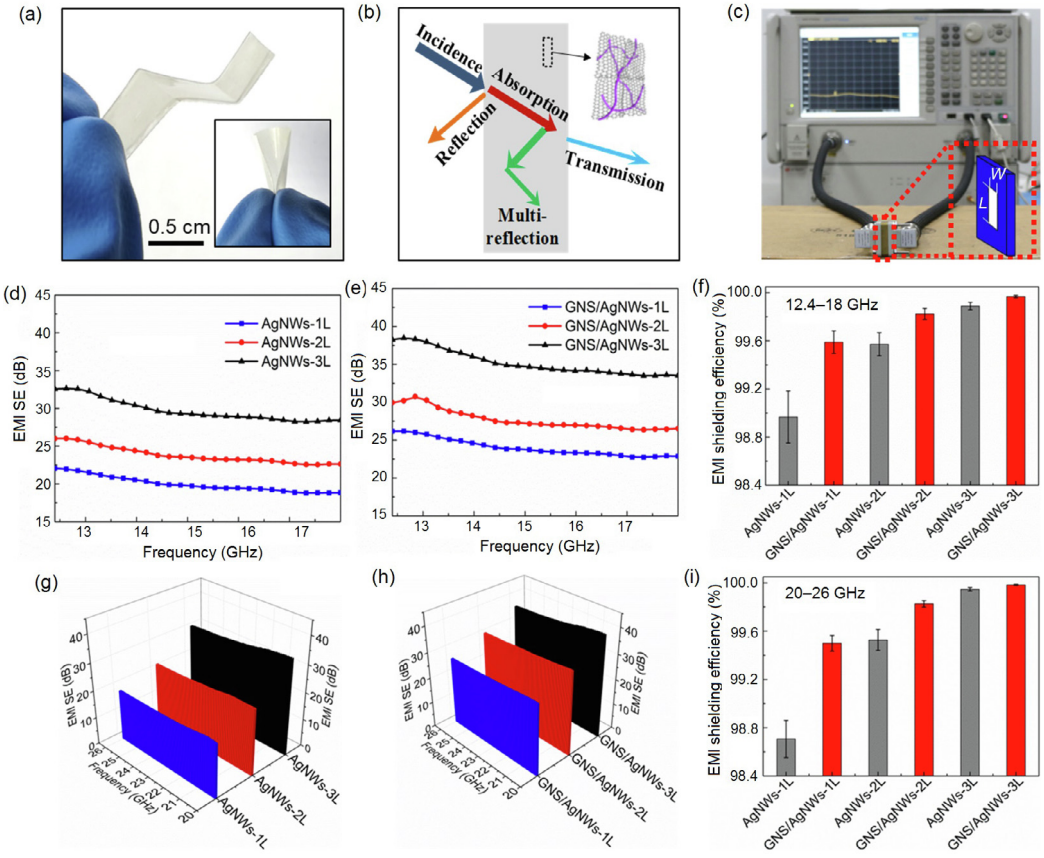

Fig. 4. (Color online) The EMI SE of the AgNWs films and GNS/AgNWs films. (a) The digital photo of flexible GNS/AgNWs films. (b) Schematic diagram of EMI shielding mechanism of the GNS/AgNWs film. (c) The digital photo of EMI SE measurement system, and the inset is a partial enlarged view of the waveguide device. *W* is the width of the film and *L* is the length of the film. The EMI SE of different content of AgNWs films (d) and GNS/AgNWs films (e) at 12.4–18 GHz, respectively. (f) The EMI shielding efficiency of different content of AgNWs films and GNS/AgNWs films at 12.4–18 GHz. The EMI SE of different content of AgNWs films (g) and GNS/AgNWs films at 20–26 GHz (h), respectively. (i) The EMI shielding efficiency of different content of AgNWs films and GNS/AgNWs films at 20–26 GHz.

at 12.4–18 GHz are shown in Figs. S5 and S6 (online), respectively. Fig. 4g, h shows that with the same AgNWs content, GNS/AgNWs films possess higher EMI SE than AgNWs films in the K-band, which exhibits the same trend as that in Ku-band. Fig. 4i shows that the EMI shielding efficiency of GNS/AgNWs film is higher than that of AgNWs film at the 20–26 GHz. The EMI shielding efficiency of GNS/AgNWs films can reach more than 99.5%, and its error is smaller than that of AgNWs films. The reflection efficiency and absorption efficiency of AgNWs films and GNS/AgNWs films at 20–26 GHz are shown in Figs. S7 and S8 (online), respectively. In addition, increasing the content of the composites, no matter AgNWs or GNS, will enhance the EMI SE. As shown in Figs. S9 and S10 (online), the EMI SE of the GO/AgNWs films in Ku-band and K-band were inferior to the GNS/AgNWs films. As shown in Table S1 (online), GNS/AgNWs films can achieve the maximum EMI SE of 40.1 dB with 47.0% light transmittance, and the maximum light transmittance of 78.4% with 28 dB EMI SE. Therefore, GNS/AgNWs films exhibit excellent EMI SE among transparent EMI shielding materials and are able to reach the balance of the EMI SE and light transmittance according to the requirement.

The EMI SE of AgNWs film and GNS/AgNWs film before and after 100 times bending were tested at 12.4–18 and 20–26 GHz. The results show that GNS/AgNWs film is more stable than AgNWs film (Fig. S11 online). Besides, the prepared AgNWs film and GNS/AgNWs film were placed in air for one month, and the EMI SE of the films were re-tested (Fig. S12 online). Fig. S12 (online) shows that the EMI SE of the AgNWs film decreases, while that of the GNS/AgNWs film remians the same. Therefore, GNS/AgNWs film possesses great flexibility and structural stability.

4. Conclusions

In conclusion, this work mainly involved the spin-coating method to prepare flexible, transparent and lightweight GNS/AgNWs film for high EMI shielding. By controlling the content of GNS, the light transmittance and EMI SE of the film can reach a balance. GNS/AgNWs films can achieve the maximum EMI SE of 40.1 dB with 47.0% light transmittance, and the maximum light transmittance of 78.4% with 28 dB EMI SE. The EMI SE and EMI shielding efficiency of GNS/AgNWs film are higher than that of AgNWs film with the same AgNWs content. At the same time, the GNS/AgNWs film has a strong flexibility and structural stability. This work provides a new research direction for transparent EMI SE, and has important scientific significance for promoting the development and realization of lightweight and high-efficiency graphene-based EMI shielding materials and smart electronics.

Conflict of interest

The authors declare that they have no conflict of interest.

Acknowledgments

This work was supported by the National Natural Science Foundation of China (51701146), the Fundamental Research Funds for the Central Universities (WUT: 2017IB015) and the Foundation of National Key Laboratory on Electromagnetic Environment Effects (614220504030617).

Author contributions

Daping He and Ning Zhang conceived and designed the experiments. Ning Zhang, Rongguo Song, Qianlong Wang, Bin Zhang, Hongye Chen, Haifei Lv and Zhi Wu carried out the experiments and discussed the results. Daping He, Ning Zhang and Zhe Wang wrote the paper. All authors commented on the manuscript.

Appendix A. Supplementary data

Supplementary data to this article can be found online at https://doi.org/10.1016/j.scib.2019.03.028.

References

[1] Singh AP, Mishra M, Sambyal P, et al. Encapsulation of γ-Fe_2O_3 decorated reduced graphene oxide in polyaniline core-hell tubes as an exceptional tracker for electromagnetic environmental pollution. J Mater Chem A 2014;2:3581–93.
[2] Shahzad F, Yu S, Kumar P, et al. Sulfur doped graphene/polystyrene nanocomposites for electromagnetic interference shielding. Compos Struct 2015;133:1267–75.
[3] Shahzad F, Alhabeb M, Hatter CB, et al. Electromagnetic interference shielding with 2D transition metal carbides (MXenes). Science 2016;353:1137–40.
[4] Fernández-García R, Gil I. Measurement of the environmental broadband electromagnetic waves in a mid-size European city. Environ Res 2017;158:768–72.
[5] Wang Z, Mao B, Wang Q, et al. Ultrahigh conductive copper/large flake size graphene heterostructure thin-film with remarkable electromagnetic interference shielding effectiveness. Small 2018;14:1704332.
[6] Chen Z, Xu C, Ma C, et al. Lightweight and flexible graphene foam composites for high-performance electromagnetic interference shielding. Adv Mater 2013;25:1296–300.
[7] Liu J, Zhang HB, Sun R, et al. Hydrophobic, flexible, and lightweight MXene foams for high-performance electromagnetic-interference shielding. Adv Mater 2017;29:1702367.
[8] Ma J, Zhan M, Wang K. Ultralightweight silver nanowires hybrid polyimide composite foams for high-performance electromagnetic interference shielding. ACS Appl Mater Interfaces 2015;7:563–76.
[9] Lee HE, Choi JH, Lee SH, et al. Monolithic flexible vertical GaN light-emitting diodes for a transparent wireless brain optical stimulator. Adv Mater 2018;30:1800649.
[10] Lee HE, Lee SH, Jeong M, et al. Trichogenic photostimulation using monolithic flexible vertical AlGaInP light-emitting diodes. ACS Nano 2018;12:9587–95.
[11] Lee HE, Lee D, Lee TI, et al. Wireless powered wearable micro light-emitting diodes. Nano Energy 2018;55:454–62.
[12] Maniyara RA, Mkhitaryan VK, Chen TL, et al. An antireflection transparent conductor with ultralow optical loss (<2%) and electrical resistance (<6 Ω/sq). Nat Commun 2016;7:13771.
[13] Batrakov K, Kuzhir P, Maksimenko S, et al. Flexible transparent graphene/polymer multilayers for efficient electromagnetic field absorption. Sci Rep 2014;4:7191.
[14] Lu Z, Wang H, Tan J, et al. Achieving an ultra-iniform diffraction pattern of stray light with metallic meshes by using ring and sub-ring arrays. Opt Lett 2016;41:1941–4.
[15] Zhu Y, Murali S, Stoller MD, et al. Carbon-based supercapacitors produced by activation of graphene. Science 2011;332:1537–41.
[16] Gupta TK, Singh BP, Mathur RB, et al. Multi-walled carbon nanotube-graphene-polyaniline multiphase nanocomposite with superior electromagnetic shielding effectiveness. Nanoscale 2014;6:842–51.
[17] Rohini R, Bose S. Electromagnetic interference shielding materials derived from gelation of multiwall carbon nanotubes in polystyrene/poly(methyl methacrylate) blends. ACS Appl Mater Interfaces 2014;6:11302–10.
[18] Sun ZW, Jin S, Jin HC, et al. Robust expandable carbon nanotube scaffold for ultrahigh-capacity lithium-metal anodes. Adv Mater 2018;30:1800884.
[19] Yousefi N, Sun X, Lin X, et al. Highly aligned graphene/polymer nanocomposites with excellent dielectric properties for high-performance electromagnetic interference shielding. Adv Mater 2014;26:5480–7.
[20] Woo Y. Transparent conductive electrodes based on graphene-related materials. Micromachines 2019;10:13.
[21] Guo W, Xu Z, Zhang F, et al. Recent development of transparent conducting oxide-free flexible thin-film solar cells. Adv Funct Mater 2016;26:8855–84.
[22] Song JZ, Xue J, Yu H, et al. Nanowire-based transparent conductors for flexible electronics and optoelectronics. Sci Bull 2017;62:143–56.
[23] Kim DG, Choi JH, Choi D, et al. Highly bendable and durable transparent electromagnetic interference shielding film prepared by wet sintering of silver nanowires. ACS Appl Mater Interfaces 2018;10:29730–40.
[24] Umrao S, Gupta TK, Kumar S, et al. Microwave-assisted synthesis of boron and nitrogen Co-doped reduced graphene oxide for the protection of electromagnetic radiation in Ku-band. ACS Appl Mater Interfaces 2015;7:19831–42.
[25] Shen B, Zhai W, Zheng W. Ultrathin flexible graphene film: an excellent thermal conducting material with efficient EMI shielding. Adv Funct Mater 2014;24:4542–8.
[26] Peng H, Dang W, Cao J, et al. Topological insulator nanostructures for near-infrared transparent flexible electrodes. Nat Chem 2012;4:281–6.
[27] Tan J, Lu Z. Contiguous metallic rings: an inductive mesh with high transmissivity, strong electromagnetic shielding, and uniformly distributed stray light. Opt Express 2007;15:790–6.
[28] Han Y, Liu YM, Liu B, et al. Optical-transparent Wi-Fi bandpass mesh-coated frequency selective surface. Electron Lett 2014;50:381–3.
[29] Jin J, Lee J, Jeong S, et al. High-performance hybrid plastic films: a robust electrode platform for thin-film optoelectronics. Energy Environ Sci 2013;6:1811–7.
[30] Vishwanath SK, Kim DG, Kim J. Electromagnetic interference shielding effectiveness of invisible metal-mesh prepared by electrohydrodynamic jet printing. Jpn J Appl Phys 2014;53:05HB11.
[31] He H, Gao C. Supraparamagnetic, conductive, and processable multifunctional graphene nanosheets coated with high-density Fe_3O_4 nanoparticles. ACS Appl Mater Interfaces 2010;2:3201–10.
[32] Dong Y, Wu ZS, Ren W, et al. Graphene: a promising 2D material for electrochemical energy storage. Sci Bull 2017;62:724–40.
[33] Novoselov KS, Geim AK, Morozov SV, et al. Electric field effect in atomically thin carbon films. Science 2004;306:666–9.
[34] Wu H, Kong D, Ruan Z, et al. A transparent electrode based on a metal nanotrough network. Nat Nanotechnol 2013;8:421–5.
[35] Hong SK, Kim KY, Kim TY, et al. Electromagnetic interference shielding effectiveness of monolayer graphene. Nanotechnol 2012;23:455704.
[36] Liu BT, Kuo HL. Graphene/silver nanowire sandwich structures for transparent conductive films. Carbon 2013;63:390–6.
[37] Kim S, Oh JS, Kim MG, et al. Electromagnetic interference (EMI) transparent shielding of reduced graphene oxide (RGO) interleaved structure fabricated by electrophoretic deposition. ACS Appl Mater Interfaces 2014;6:17647–53.
[38] Sun C, Bai B. Molecular sieving through a graphene nanopore: non-equilibrium molecular dynamics simulation. Sci Bull 2017;8:34–42.
[39] Han Y, Liu Y, Han L, et al. High-performance hierarchical graphene/metal-mesh film for optically transparent electromagnetic interference shielding. Carbon 2017;115:34–42.
[40] Ma L, Lu Z, Tan J, et al. Transparent conducting graphene hybrid films to improve electromagnetic interference (EMI) shielding performance of graphene. ACS Appl Mater Interfaces 2017;9:34221–9.
[41] Lu Z, Ma L, Tan J, et al. Graphene, microscale metallic mesh, and transparent dielectric hybrid structure for excellent transparent electromagnetic interference shielding and absorbing. 2D Mater 2017;4:025021.
[42] Karagiannidis PG, Hodge SA, Lombardi L, et al. Microfluidizationof graphite and formulation of graphene-based conductive inks. ACS Nano 2017;11:2742.
[43] Yang C, Gu H, Lin W, et al. Silver nanowires: from scalable synthesis to recyclable foldable electronics. Adv Mater 2011;23:3052–6.
[44] Song R, Wang Q, Mao B, et al. Flexible graphite films with high conductivity for radio-frequency antennas. Carbon 2018;130:164–9.
[45] Buechel D, Mihalcea C, Atoda N, et al. Raman spectroscopic investigation of reactively sputtered silver oxide layers: a ready-made silver nanocluster precursor for optical plasmon generation. Proc SPIE 2001;4469:85–92.
[46] Kim F, Luo J, Cruz-Silva R, et al. Self-propagating domino-like reactions in oxidized graphite. Adv Funct Mater 2010;20:2867–73.
[47] Chen Y, Zhang HB, Yang Y, et al. High-performance epoxy nanocomposites reinforced with three-dimensional carbon nanotube sponge for electromagnetic interference shielding. Adv Funct Mater 2015;26:447–55.
[48] Jia LC, Yan DX, Cui CH, et al. Electrically conductive and electromagnetic interference shielding of polyethylene composites with devisable carbon nanotube networks. J Mater Chem C 2015;3:9369–78.
[49] Tan L, Zeng M, Wu Q, et al. Direct growth of ultrafast transparent single-layer graphene defoggers. Small 2015;11:1840–6.

Ning Zhang received the B.S. degree in Electronic Information Science and Technology from the Wuhan University of Technology in 2016. Currently, she is pursuing the M.S. degree in physics at School of Science, Wuhan University of Technology. Her research interests include conductive graphene films and transparent electromagnetic shielding material.

Daping He is a full professor at Wuhan University of Technology. He obtained his Ph.D. degree in Materials Processing Engineering from Wuhan University of Technology in 2013. He was a Postdoctoral Fellow in the University of Science and Technology of China. Then he joined University of Bath as a Newton International Fellow and University of Cambridge as a Postdoctoral Fellow. His research interest is preparation and application of nano composite materials into new energy devices, sensors and RF microwaves field.